Acta Materialia 223 (2022) 117465

Contents lists available at ScienceDirect

Acta Materialia

journal homepage: www.elsevier.com/locate/actamat

Full length article

Electric-field-induced annihilation of localized gap defect states in amorphous phase-change memory materials

Konstantinos Konstantinou[a,1,*], Felix C. Mocanu[b], Jaakko Akola[c,d], Stephen R. Elliott[a,2]

[a] Department of Chemistry, University of Cambridge, Cambridge CB2 1EW, UK
[b] Department of Engineering, University of Cambridge, Cambridge CB3 0FF, UK
[c] Computational Physics Laboratory, Faculty of Engineering and Natural Sciences, Tampere University, Korkeakoulunkatu 3, Tampere FI-33014, Finland
[d] Department of Physics, Norwegian University of Science and Technology (NTNU), Trondheim NO-7491, Norway

ARTICLE INFO

Article history:
Received 1 August 2021
Revised 27 October 2021
Accepted 2 November 2021
Available online 6 November 2021

Keywords:
Phase-change memory
Amorphous materials
Electric field
Defects
First-principles calculations

ABSTRACT

Structural relaxation of amorphous phase-change-memory materials has been attributed to defect-state annihilation from the band gap, leading to a time-dependent drift in the electrical resistance, which hinders the development of multi-level memory devices with increased data-storage density. In this computational study, homogeneous electric fields have been applied, by utilizing a Berry-phase approach with hybrid-density-functional-theory simulations, to ascertain their effect on the atomic and electronic structures associated with the mid-gap states in models of the prototypical glassy phase-change material, $Ge_2Sb_2Te_5$. Above a threshold value, electric fields remove spatially localized defects from the band gap and transform them into delocalized conduction-band-edge electronic states. A lowering of the nearest-neighbor coordination of Ge atoms in the local environment of the defect-host motif is observed, accompanied by a breaking of 4-fold rings. This engineered structural relaxation, through electric-field tuning of electronic and geometric properties in the amorphous phase, paves the way to the design of optimized glasses.

1. Introduction

The future of energy-efficient computing will increasingly move from being computer-centric to being memory-centric. The rapid development of big-data analytics and artificial intelligence demands a fundamental change in the current computing systems, which are based on a von Neumann architecture; therefore, novel data-storage and data-processing technologies are under intense development nowadays [1,2]. The concept of storage-class memory (SCM) has been put forward, based on emerging ultra-low-power, non-volatile memory technologies, to bridge the gap of rapid access time between memories and data-storage systems [3].

Phase-change random-access memory (PCRAM) is a novel technology that is currently used in the Optane™ SCM product, since it features great scaling potential (down to a few nm), implementation in 3D, reliability, low cost and simplicity [4]. In PCRAM devices, non-volatile data storage is based on the metastable structural phases of a chalcogenide memory material, with the digital information being encoded through reversible and rapid ('phase-change') transformations between a low-resistance crystalline phase (the "1-bit") and a high-resistance glassy phase (the "0-bit") by the application of suitable electrical pulses [5]. Ge-Sb-Te chalcogenide alloys display an ultra-fast (~ ns) crystallization, that is appropriate for PCRAM technology, and currently, the canonical composition, $Ge_2Sb_2Te_5$ (GST-225), is utilized as the core material for PCRAM programming [6].

A spontaneous structural relaxation of the amorphous state ("aging") created via a melt-and-quench process is evident in all types of glassy materials [7]. The timescale of this process varies by several orders of magnitude among different glasses. In phase-change materials, it can take place rather quickly and it has been identified as being a potential source of the undesirable time-dependent increase in electrical resistance ("drift") in PCRAM devices [8], which threatens the development of multi-level storage in such non-volatile memories.

Upon structural relaxation, the amorphous (glassy) phase evolves with time towards an energetically favorable glassy state [9]. During this process, one would expect in-gap defect states

* Corresponding author.
E-mail address: konstantinos.konstantinou@tuni.fi (K. Konstantinou).
[1] Present address: Computational Physics Laboratory, Faculty of Engineering and Natural Sciences, Tampere University, Korkeakoulunkatu 3, Tampere FI-33014, Finland
[2] Present address: Physical and Theoretical Chemistry Laboratory, University of Oxford, Oxford OX1 3QZ, UK.

https://doi.org/10.1016/j.actamat.2021.117465

to disappear gradually with time, in order to reduce the overall free energy of the system, thus resulting in more energetically stable structures, and hence leading to an increase of the resistance [10,11]. Experimental studies on glassy GeTe have indicated a shift of the in-gap defects and band edges away from the Fermi level upon structural relaxation, simply owing to a stretching of the density of states, which also leads to a movement of the Fermi level nearer to mid-gap [12–14].

The annealing of coordination defects in amorphous phase-change materials is a very slow process, and, therefore, a complex task to simulate. The structural relaxation of amorphous GeTe has been studied by chemical substitution [15] and by metadynamics [16]. These studies show that the relaxation of the glass breaks Ge–Ge bonds, favoring three-fold coordinated Ge and Te atoms and p-bonding type, while also an increase of the band gap of the glass was observed. In another modeling study of amorphous GeTe, replica-exchange molecular-dynamics simulations were employed, together with first-principles calculations [17]. The authors indicated a correlation between the structural relaxation (and hence the resistance increase) and the annihilation of structural defects responsible for localized electronic states, which occurs via a lowering of the Ge coordination and a series of collective rearrangements of the defect complexes [17,18].

Fantini et al. reported experimentally that resistance drift (and hence structural relaxation) in the amorphous state of phase-change memory materials can be accelerated by the application of an external electric field to the memory cell [19]. In addition, a kinetic model that describes the amorphous network in terms of many two-level systems with distributed activation energies was utilized to interpret their experimental measurements. Then, their findings were explained by considering the energy-barrier-lowering effect induced by the external bias on the ensemble of the two-level systems to lower the internal total energy of the system over time [19]. However, it should be noted that such physical modeling does not account for the electronic structure of the glassy material and the presence of defect-related localized electronic states inside the band gap, as well as at the band tails, which are known to be present in amorphous phase-change memory materials (and an intrinsic property of any disordered non-metallic material [20]), and which can affect resistance drift [10,12,13].

In our recent work [21], using hybrid density-functional-theory simulations, we identified and characterized the atomic (geometric) and electronic structures of the mid-gap electronic states in an ensemble of 30 models of amorphous GST-225, generated using a machine-learned, Gaussian Approximation Potential [22]. The calculations demonstrated that 5-coordinated Ge atoms are the dominant local defective bonding environments which are mostly responsible for hosting the mid-gap electronic states [21]. The analysis revealed that the mid-gap defect states are strongly spatially localized on crystalline-like atomic fragments within the amorphous network, consisting of groups of high-coordination Ge atoms and 4-fold ring structures [21]. It is noted that 4-fold rings have been previously identified as an essential feature of the amorphous structure of GST-225 [23,24].

We note that localized gap states (strictly) related to Ge–Ge bonds, similar to those which have been identified in the binary material, amorphous GeTe [15,16], are absent from our GST-225 amorphous models. This is probably due to the under-estimation of the amount of homopolar bonds and the proportion of tetrahedral Ge environments in the GAP-generated glass structures compared with DFT-generated models [22]. Nevertheless, it is important to highlight that, even though GeTe is a material that is a parent phase of GST-225, it has a much simpler structure compared to the complex atomic environments of the ternary GST-225 material, which implies that the atomic geometries of the localized mid-gap defect states in GST-225 might differ from those observed for the relevant defects in amorphous GeTe. Moreover, the model structures generated with the GAP potential are not missing any of the atomic environments believed to be present in amorphous GST-225, and they can be indeed representative of the glass [21,22].

It is well established that structural relaxation of the glassy phase involves the breaking of bonds and rearrangement of the structure, which can be an extremely slow process. In this study, we aim to achieve a fundamental understanding, at the atomistic level, of the effect that an applied electric field has on the spatial localization and atomic character of the mid-gap defect electronic states in glassy phase-change-memory materials. We utilize a Berry-phase approach to include an external electric field, combined with density-functional theory (DFT) calculations using non-local exchange-correlation functionals, in order to explore its effect on the position of the in-gap states in the band gap, their degree of spatial localization, and the local atomic environments which host them.

In this way, we provide an accurate picture of the interplay between an electric field and defect states in the band gap of the glassy state of the GST-225 phase-change-memory material. We demonstrate how an external electric field can be used to engineer defect annihilation in amorphous phase-change materials, and we highlight this as an example of electric-field tuning of electronic behavior in glasses.

2. Computational details

An ensemble of 30 independent, amorphous 315-atom supercell GST-225 models was generated following a melt-and-quench approach, by classical molecular-dynamics simulations employing a machine-learned, Gaussian Approximation Potential for Ge-Sb-Te materials [21]. The atomic geometry of the model glassy structures was further optimized using DFT calculations, and the electronic structure of the glassy models was calculated in order to identify and characterize the mid-gap electronic states, and hence to obtain a statistically significant understanding about these defects present in the band gap of the amorphous material. Details about these simulations, the quality of the generated amorphous models and the intrinsic nature of the mid-gap defect states can be found in our previous work [21].

In this study, in order to simulate the effect of an external electric field on the atomic geometry and electronic structure of amorphous GST-225, model structures that exhibit defect-related electronic states within the band gap were selected from the ensemble database. In particular, three glass model structures were examined in detail: *M1* with a well-defined mid-gap defect state, *M2* with a shallow defect state, and *M3* with two defect states within the band gap.

The Berry-phase approach, within the modern theory of polarization [25–28], was employed to compute the effect of an applied periodic electric field on in-gap defect states in the GST-225 amorphous models. In order to study the impact of the intensity of the external electric field, seven different field strengths were applied, varying by intervals of 500 kV cm^{-1}, viz. 500, 1000, 1500, 2000, 2500, 3000 and 3500 kV cm^{-1}. The effect of the direction of the polarization vector of the external electric field was investigated by applying two different intensities of electric fields (500 and 2500 kV cm^{-1}) along seven different directions within the cubic simulation cell containing the model amorphous network, namely ⟨001⟩, ⟨010⟩, ⟨100⟩, ⟨110⟩, ⟨101⟩, ⟨011⟩ and ⟨111⟩.

Density-functional theory (DFT), as implemented in the CP2K code [29], was used to optimize the geometries of the amorphous GST-225 structures, under the application of an external electric field, and to calculate their electronic properties. The CP2K code uses a mixed Gaussian basis set with an auxiliary plane-

wave basis set to represent the electrons in the modeled system [30]. Periodic-boundary conditions were enforced in all the calculations. All atomic species were represented using a double-ζ valence-polarized (DZVP) Gaussian basis set [31], in conjunction with the Goedecker-Teter-Hutter (GTH) pseudopotential [32]. The plane-wave energy cut-off was set to 400 Ry. The atomic geometry of the glass models, under the application of an external periodic electric field, was optimized, and the electronic structure was calculated by using the non-local PBE0 functional [33]. We note that the amount of exact exchange and the cut-off radius of this hybrid functional can be adjusted to achieve an optimal accuracy for the electronic structure of the particular system under study. In this work, an amount of 25% for the Hartree-Fock exchange, with a cut-off radius of 3 Å for the truncated Coulomb operator, were employed. The inclusion of the Hartree-Fock exchange with this specific parametrization provides a more accurate description of the band gap and the localized defect states in our GST-225 glass models [21,34]. The computational cost of hybrid-functional calculations was reduced by using the auxiliary density-matrix method (ADMM) [35], as successfully employed in several previous modeling studies of amorphous materials [21,34,36,37].

The Broyden-Fletcher-Goldfarb-Shanno (BFGS) algorithm was applied in the geometry optimizations of the amorphous structures in order to minimize the total energy of the modeled systems. The BFGS corresponds to a local-search optimization algorithm, which implies that, in this process, the geometry optimizer moves "downhill" on the potential-energy surface into the local minimum. The convergence criterion for the forces on atoms of the current configuration in an iteration step was 0.023 eV Å^{-1}, while the root-mean-square (RMS) force was required to be smaller than 2/3 of the maximum force. Moreover, the change in the total energy of the glass model between the final optimized geometry and the second-to-last iteration of the calculation was minimized to within 10^{-4} eV. A detailed description on the working principle of the BFGS algorithm is given in the Supplementary Materials.

3. Results and discussion

3.1. Effect of an electric field on the electronic structure

The effect of the intensity of the applied electric field on the mid-gap electronic states was investigated by applying field strengths ranging from 500 to 3500 kV cm^{-1}, in 500 kV cm^{-1} intervals, along the same body-diagonal direction, ⟨111⟩, within the cubic supercells containing the model amorphous networks. Periodic spin-polarized hybrid-DFT calculations were employed to optimize the geometry of the glass structures, under the application of an external electric field, and to calculate their electronic structure.

The total and partial electronic densities of states (DOS, PDOS, respectively) of the glass model *M1*, before and after the application of a high external electric field, are shown in Fig. 1(a). The electronic-structure calculations show a band gap of 0.6 eV for the relaxed ground state, while the unoccupied mid-gap defect state is located at 0.27 eV below the bottom of the conduction band. In Fig. 1(a) (bottom panel), it can be observed that the application of a 2500 kV cm^{-1} electric field eliminates the mid-gap defect state from the electronic structure of the glass model, transforming it into a conduction-band-minimum electronic state; this results in a Kohn-Sham band gap of 0.66 eV, slightly larger than that of the zero-field glass structure. The calculated value of the band gap agrees very well with the experimentally reported values for amorphous GST-225, ranging between 0.6 and 0.8 eV [38,39]. Before the application of the electric field, the mid-gap defect state is dominated by the contribution from Te-atom states, with a contribution also from Ge-atom states, while the Sb contribution is almost negligible (see top panel in Fig. 1(a)). In contrast, after the application of the high electric field, the Sb contribution becomes more significant for this electronic state, which now resides at the bottom of the conduction band (see bottom panel in Fig. 1(a)).

The energy position of the Fermi level in the total electronic densities of states of the GST-225 glass model *M1*, for all the different applied electric fields, is shown in Fig. 2(a). The Fermi level lies deep in the band gap, between the mid-gap electronic state and the valence-band maximum, in the original, zero-field GST-225 amorphous model. It can be observed that the Fermi level moves towards the conduction-band edge (higher-energy values) with increasing electric-field intensity (as also shown in Fig. 2(b) where the evolution of the Fermi level versus the intensity of the applied electric field is presented), but, at the same time, the HOMO-LUMO band gap is slightly changing as well. After the application of a 2500 kV cm^{-1} electric field, the mid-gap state has been removed from the band gap of the glass, while the Fermi level now lies approximately in the middle of the band gap.

In order to highlight the significance of atomic relaxation of the amorphous model, due to the application of an electric field, on the shift of the mid-gap state to the bottom of the conduction band, a single-point, hybrid-DFT electronic-structure calculation was performed for the GST-225 model *M1* by keeping the atoms in the simulation box fixed at the positions of the original, zero-field geometry, while applying a 2500 kV cm^{-1} electric field along the ⟨111⟩ direction. The total DOS before and after the application of the electric field shows that the mid-gap state remains intact at its energy level in the band gap of the glassy model (see **Fig. S1**), indicating that the electric field itself cannot induce the relevant elimination of the defect state, as is shown in Fig. 1(a) for the same model after the geometry optimization of the glass structure under the application of the high external electric field.

In order to determine whether the effect of an electric field on the electronic structure of amorphous GST-225, with respect to the annihilation of mid-gap defect states, is permanent (at least from the perspective of the static simulations presented herein), the geometry of the relaxed glass system after the application of the electric field was re-optimized, with a hybrid-DFT calculation, after turning off the electric field. The total DOS of the final relaxed glass structure *M1* with the applied electric field, and the subsequent geometry relaxation without the electric field, are shown in **Fig. S2(a)**. It is noteworthy that the action of the high external electric field causes an irreversible modification in the electronic structure of the glassy model, since no in-gap defect states re-appear after cessation of the applied electric field.

The same effect of an electric field on the electronic structure of amorphous GST-225 can be observed in the glassy model *M3* with two in-gap states, a mid-gap defect state and a shallower in-gap electronic state, located at 0.35 eV and 0.15 eV, respectively, below the bottom of the conduction band. The application of a 2500 kV cm^{-1} electric field eliminates both the gap electronic states, resulting in a "clean" band gap, as can be seen from a comparison between the top and bottom panels in Fig. 1(b).

The total DOS, for all the different intensities of the applied electric field for the three amorphous GST-225 models studied in this work, are shown in **Fig. S3**. For applied external electric fields with intensities up to 2000 kV cm^{-1}, the in-gap electronic states remain intact at their energy positions in the band gap of the glass. For the glass model which exhibits only a shallow in-gap electronic state (model *M2*), located at 0.17 eV below the bottom of the conduction band, an electric field higher than 3000 kV cm^{-1} was required to remove the defect state from the band gap.

We note that Zener breakdown, associated with the electric-field-induced tunneling of electrons from the valence band to the conduction band, should not occur in the simulations presented in this study. The threshold Zener-breakdown voltage for the amor-

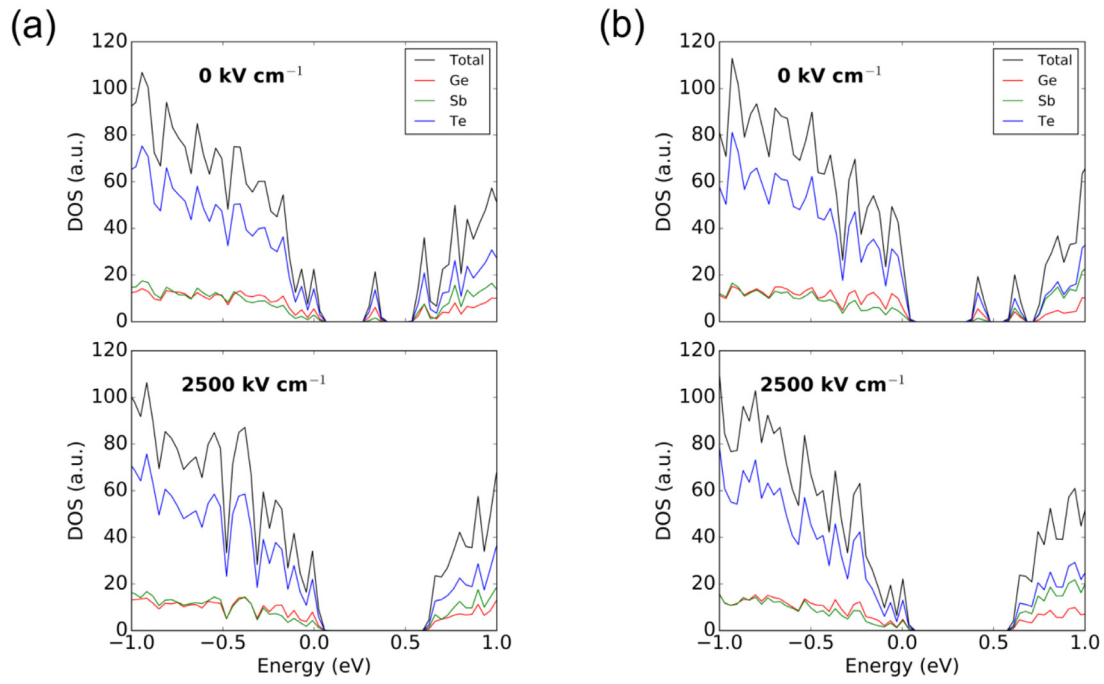

Fig. 1. Effect of an electric field on the electronic structure of glassy GST-225. Total and partial electronic densities of states (DOS/PDOS) near the top of the valence band and the bottom of the conduction band before and after the application of a 2500 kV cm^{-1} external electric field along the ⟨111⟩ direction for: (a) a GST-225 model structure with a mid-gap defect state in the band gap (model *M1*) and (b) a GST-225 model structure with two in-gap states in the band gap (model *M3*). In-gap defect states are eliminated from the electronic structure of both glass models due to the electric-field-induced atomic relaxations of the amorphous structures.

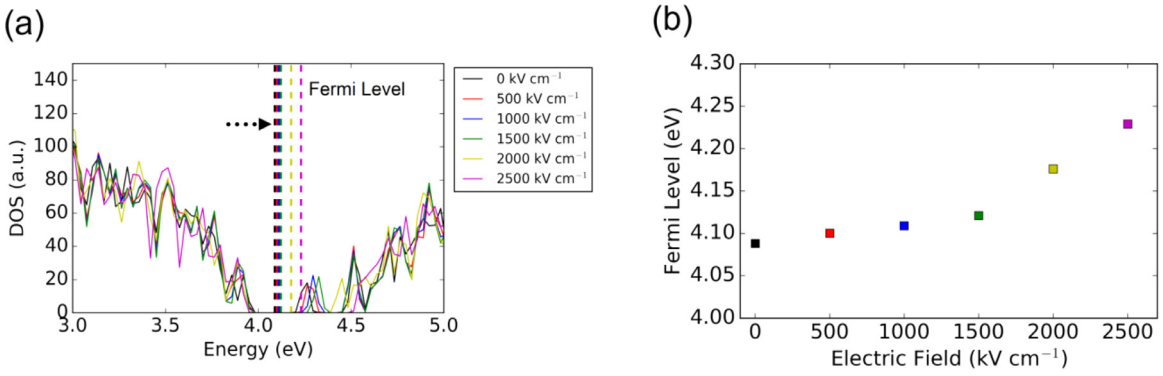

Fig. 2. Evolution of the Fermi level as a function of the applied electric field. (a) Total electronic densities of states (DOS) near the top of the valence band and the bottom of the conduction band for the GST-225 glass model *M1*, originally with a mid-gap defect state, after the application of periodic electric fields ranging from 500 to 2500 kV cm^{-1} along the ⟨111⟩ direction. The position of the Fermi level in the band gap of the modeled system is indicated, in each case, with a colored dashed vertical line. (b) Energy position of the Fermi level in the band gap of the glass model versus the intensity of the applied electric field. The Fermi level moves towards the conduction-band edge with increasing electric-field intensity.

phous GST-225 models studied here, with a band-gap energy of ∼ 0.6 eV, would be ∼ 2.4 V ($V_Z \sim 4\ E_g/e$) [40]. The voltage across the 2.2 nm cubic simulation cell of the model glassy structures, corresponding to an observed typical threshold electric field of 2500 kV cm^{-1}, is 0.55 V, smaller even than the band-gap potential value itself. Moreover, Zener breakdown should not be involved in the observed field-induced behavior of the mid-gap defect states, since the electronic states that are eliminated from the band gap are *unoccupied*, so that there are no electrons in such levels able to tunnel to the conduction band.

3.2. Effect of an electric field on electron localization

In glass model *M1*, electric fields above a threshold intensity of ∼ 1500 kV cm^{-1}, viz. 2000 kV cm^{-1} and 2500 kV cm^{-1}, remove the mid-gap electronic state from the band gap, as can be observed in Figs. 1 and **S3**, essentially transforming it into a conduction-band-edge electronic state. It has been established that the mid-gap defect states are strongly spatially localized in the glassy GST-225 model structure [21]. In order to examine, quantitatively, the effect of an applied external electric field on the degree of spatial localization of the mid-gap electronic state, as well as of each single-particle Kohn-Sham state in the electronic structure of the amorphous model *M1*, the inverse participation ratio (IPR) was calculated for each value of electric-field intensity, ranging from 0 to 2500 kV cm^{-1}. We note that this IPR method has been previously widely used to characterize the localization of vibrational and electronic states in amorphous materials [41–44].

The IPR spectrum near the valence- and conduction-band edges for the GST-225 glass model *M1*, before and after the application of the 2500 kV cm^{-1} electric field, is shown in the top panels of Fig. 3**(a)** and **3(b)**, respectively. One can clearly observe that the mid-gap defect state is fairly strongly localized, with an IPR value of ∼ 0.05. The application of an above-threshold external electric

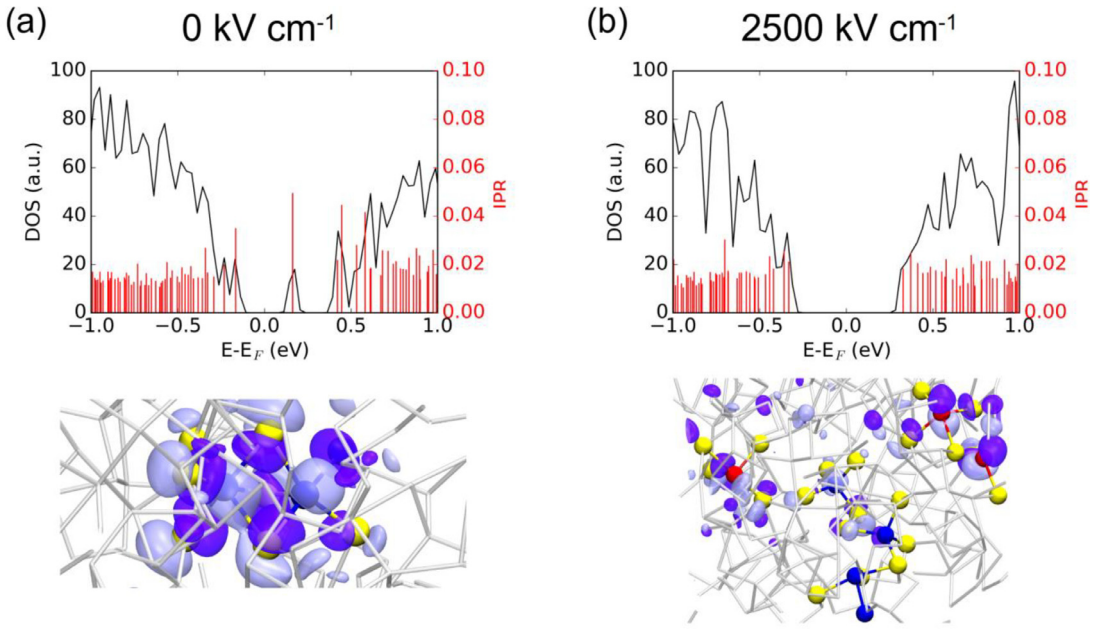

Fig. 3. Effect of an electric field on electron localization. *Top panels*: Total electronic density of states (DOS–black solid line), near the top of the valence band and the bottom of the conduction band of the amorphous GST-225 model *M1*: (a) before; and (b) after the application of a 2500 kV cm^{-1} external electric field along the ⟨111⟩ direction. The corresponding values of the inverse participation ratio (IPR) for the Kohn-Sham orbitals are highlighted with red spikes. *Bottom panels*: Molecular orbitals of the original mid-gap defect state (left), and the corresponding electronic state shifted to the bottom of the conduction band after the application of the electric field (right). The 2500 kV cm^{-1} electric field transforms the localized mid-gap defect state into a delocalized conduction-band-minimum electronic state. Ge atoms are blue, Sb are red, and Te are yellow. The atomic bonds in the rest of the amorphous network are rendered in gray. The purple and blue isosurfaces, in both configurations, depict the molecular-orbital-wavefunction amplitude of the respective electronic state, and are plotted with isovalues of +0.015 and -0.015, respectively (For interpretation of the references to color in this figure legend, the reader is referred to the web version of this article).

field reduces dramatically the spatial localization of the previously mid-gap defect state, which now lies at the bottom of the conduction band, resulting in an IPR value of ∼0.02; essentially, it cannot be considered as a localized defect state anymore. In addition, the applied electric field causes a decrease in the degree of localization of every electronic state near the tail of the conduction band, resulting in a near-constant IPR value throughout the conduction band, together with an almost linear conduction-band edge in the DOS of the glass model, while a similar effect is also observed in the valence band. **Fig. S2(b)** shows that the delocalization of the electronic states at the band edges remains unchanged after cessation of the applied external electric field.

The bottom panels of Fig. 3**(a)** and **(b)** show the molecular orbitals of the original, zero-field mid-gap electronic state, and of the translated electronic state at the bottom of the conduction band after the application of an electric field with an intensity of 2500 kV cm^{-1}, respectively. The strongly localized character of the original mid-gap defect state has been lost, since the translated conduction-band-edge electronic state becomes delocalized within the amorphous network, clearly highlighting the marked effect of above-threshold electric fields on the degree of spatial localization.

Clima et al. showed, using DFT simulations, combined with a Berry-phase approach, that the application of a strong electric field results in wider conduction-/valence-band tails in amorphous GeSe-based selector materials [45]. They argued that the applied electric field can lead to delocalization of tail- and mobility-gap-states, as well as to some sort of charge-carrier re-population [45].

The IPR spectra for applied sub-threshold electric fields, of intensities 500, 1000, 1500 and 2000 kV cm^{-1}, for the glass model *M1*, are shown in **Fig. S4**. It can be observed that, for values of electric field up to 2000 kV cm^{-1}, the mid-gap defect state maintains its strongly localized character. It is interesting to highlight that for the 2000 kV cm^{-1} electric field, even though the mid-gap state has been moved to the bottom of the conduction band, the IPR value indicates that it is still a rather localized electronic state, suggesting that it corresponds to a defect state in the tail of the conduction band.

The evolution of the IPR value of the electronic state, which was originally a mid-gap state in glass model *M1*, versus the intensity of the applied electric field is presented in **Fig. S5**; it can be observed that the electronic state remains localized within the amorphous network for values of electric field up to 2000 kV cm^{-1}, whereas extensive delocalization of the electronic state is indicated by the remarkable drop of the IPR value for the 2500 kV cm^{-1} applied external electric field.

The significant threshold electric-field-induced delocalization of the electronic states in the tail of the conduction (and valence) band of the simulated amorphous GST-225 model could have implications related to the electrical conductivity of the glassy material. This observation resembles the model proposed by Lebedev and Rogachev to explain threshold switching in chalcogenide glasses [46] (a breakdown in electronic resistance by three orders of magnitude in amorphous GST-225, for instance [47]), wherein it is presumed that an electric field can decrease the energies of localized tail states in the band gap, and even destroy them if they are shallow enough, except that we find that high electric fields can effectively eliminate and delocalize even mid-gap states, as well as tail states. However, we note that such a correlation, at the atomistic level, would require further (transport) calculations in order to confirm it.

3.3. Local atomic structure and delocalization

Structural modifications in the atomic geometries, that host localized mid-gap defect states eliminated due to an applied high electric field, can be highlighted through a direct visualization of the relevant wavefunctions in the GST-225 glass models.

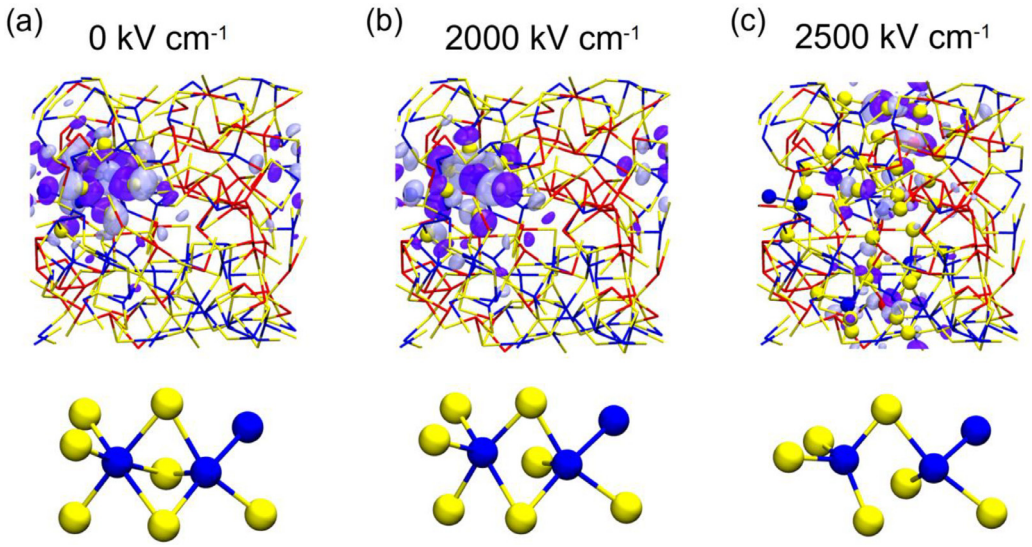

Fig. 4. Correspondence of the atomic geometry and the degree of electron localization. Atomic structure and molecular orbital of: (a) The original mid-gap electronic state in the band gap of the zero-field glassy GST-225 model *M1*. (b) The electronic state after the application of a 2000 kV cm^{-1} electric field along the ⟨111⟩ direction. (c) The electronic state after the application of a 2500 kV cm^{-1} electric field along the ⟨111⟩ direction. The localization of the electronic state is correlated with the atomic geometry that is acting as host, which can be influenced by the application of a suitable external electric field. Ge atoms are blue, Sb are red, and Te are yellow. The bonds in the rest of the amorphous network are rendered as sticks, colored according to the type of atoms involved in the bonding. The purple and blue isosurfaces, in every configuration, depict the molecular-orbital-wavefunction amplitude of the relevant electronic state, and are plotted with isovalues of +0.015 and -0.015, respectively (For interpretation of the references to color in this figure legend, the reader is referred to the web version of this article).

The molecular orbital of the mid-gap electronic state in glass model *M1*, before the application of an electric field, is shown in the upper panel of Fig. 4**(a)**. One 5-coordinated Ge atom and one 6-coordinated Ge atom form the local atomic environment in which the mid-gap defect state is localized in the amorphous network (lower panel). In addition, a Ge–Te–Ge–Te 4-fold ring contributes to the picture of the host structural motif for the mid-gap defect state. It is noted that these observed local environments are in accordance with the previous findings from an ensemble of thirty GST-225 model structures [21].

After the application of the 2000 kV cm^{-1} external electric field, we observed that the mid-gap electronic state was removed from the band gap and appeared at the bottom of the conduction band. Nevertheless, the degree of spatial localization of the newly formed electronic state remained very strong (**Figs. S4** and **S5**). The molecular orbital of the electronic state in this case, shown in the upper panel of Fig. 4**(b)**, reveals that the atomic geometry that hosts the localized state has changed only slightly from the atomic geometry of the original, zero-field mid-gap defect state. The initially 6-coordinated Ge atom becomes 5-coordinated, while the other Ge atom, in the motif of the defect, maintains its 5-fold coordination, and the 4-fold ring structure remains intact (lower panel). This is an indication that, even though the high electric field removed the mid-gap defect from the band gap, the localization of the electronic state is strongly connected to the relevant atomic geometry, and in particular to the local environment of the 5-coordinated Ge atoms and the 4-fold ring structure, distinctive for the mid-gap electronic states in GST-225 [21].

A subsequent increase in the intensity of the applied electric field, viz. to 2500 kV cm^{-1}, leads to complete delocalization of the conduction-band-edge state (**Fig. S5**). In order to examine how this translates to any possible modification of the atomic environment that was hosting the mid-gap defect, the wavefunction of the molecular orbital for this case is shown in the upper panel of Fig. 4**(c)**. It can be clearly observed that the local atomic environments of the two Ge atoms that were involved in the localization of the zero-field, mid-gap defect state in glass model *M1* have been transformed, after the application of the 2500 kV cm^{-1} electric field, from being 5- and 6-coordinated to both being 4-coordinated, while also one of the Ge–Te bonds in the original 4-fold ring is broken (lower panel). In an extended view of the molecular orbital, it can be seen that the electronic state is no longer localized on the initial atomic motif, but instead it is now delocalized in the periodic cell of the GST-225 glass structure, involving several Sb and Ge atoms with 3- and 4-coordinated local environments.

The correlation between the applied electric field, the transformation of a mid-gap defect state to a conduction-band-edge state, and the change in the degree of its localization and the atomic geometry which hosts the localized mid-gap electronic state, is also found in the case of the GST-225 glass model *M3*. The original mid-gap defect state is localized on an atomic fragment that consists of a small group of four Ge atoms, of which three are 5-coordinated and one is 4-coordinated, as shown in **Fig. S6(a)**. The application of a 2500 kV cm^{-1} electric field removes both the in-gap states from the band gap, while the mid-gap defect now lies at the bottom of the conduction band. All of the previously 5-coordinated Ge atoms in the structural motif of the electronic state become 4-coordinated, while the previously 4-coordinated Ge atom becomes 3-coordinated, as can be seen in **Fig. S6(b)**.

The field-induced atomic displacements for the three component species (Ge, Sb and Te) were calculated in the glass model *M1* to investigate how changes in the atomic geometry correlate with the transformation of a localized mid-gap defect state to a delocalized conduction-band-edge state under the application of the 2500 kV cm^{-1} external electric field along the ⟨111⟩ direction. The local atomic structure hosting the delocalized electronic state (after), which lies at the bottom of the conduction band, differs, on average, from that hosting the localized mid-gap electronic state (before) by 0.14 Å, 0.08 Å and 0.11 Å displacements of the Ge, Sb, and Te atoms, respectively.

The individual displacements of all the 315 atoms in glass model *M1* are presented as a function of the distance of each atom from the center of mass of the mid-gap defect state in Fig. 5**(a)**, and they provide information on the spatial range of displacements of the atoms within the glass network due to the application of the 2500 kV cm^{-1} electric field. Clearly, the atoms that experienced

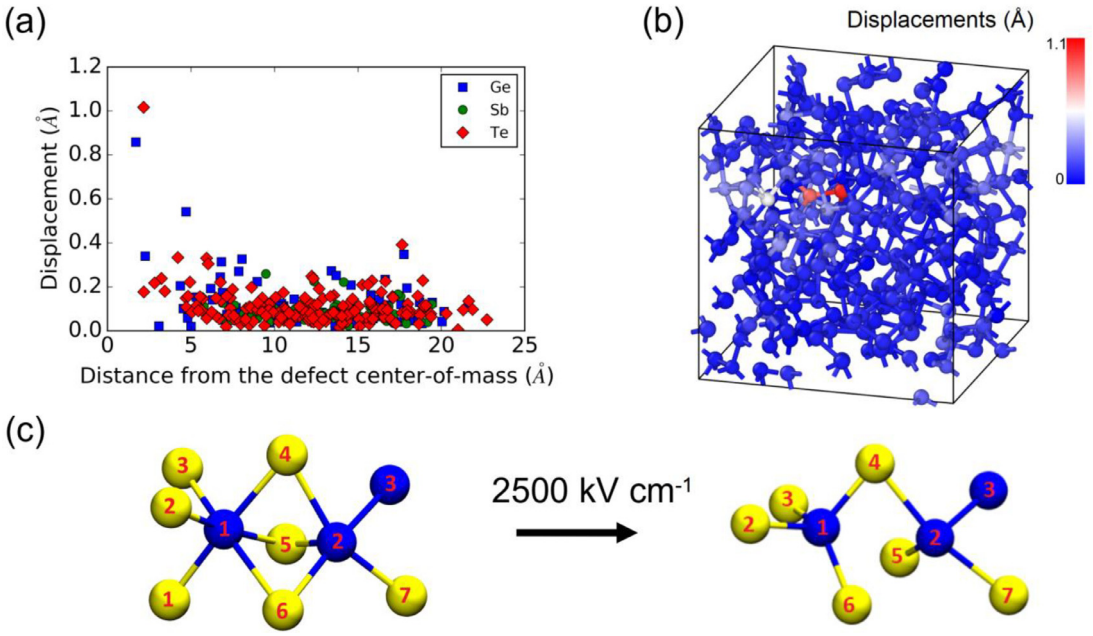

Fig. 5. Effect of an electric field on the atomic displacements. (a) Atomic displacements for Ge, Sb and Te atoms in the relaxed amorphous GST-225 structure *M1* after the application of an electric field (2500 kV cm^{-1}, ⟨111⟩ direction), as a function of the distance of each atom from the center-of-mass of the mid-gap defect. (b) Visualization of the distribution of atomic displacements for all the 315 atoms in the glass model *M1* after the application of the high electric field. The color palette between blue and red indicates the value of the atomic displacement and ranges from 0 to 1.1 Å. (c) Local environment of the two Ge atoms that correspond to the atomic motif that hosts the localized mid-gap defect state of the glassy model *M1* before the application of an electric field (left) and the local environment of the same two Ge atoms after the application of the 2500 kV cm^{-1} electric field along the ⟨111⟩ direction (right). Ge atoms are blue and Te are yellow. Atoms that participate in the structural motif of the defect experience large displacements after the application of the external electric field (For interpretation of the references to color in this figure legend, the reader is referred to the web version of this article).

the largest displacements are those which take part in hosting the electron localization of the original mid-gap defect. In addition, the displacements of all the 315 atoms in the glass model *M1* are plotted as a color map in Fig. 5**(b)**, while Fig. 5**(c)** shows the atomic geometry of the mid-gap defect before and after application of the 2500 kV cm^{-1} electric field. The 6-coordinated Ge atom (denoted as Ge_1) that participated in the structural motif which hosted the localized mid-gap electronic state experiences a displacement of 0.86 Å, which is significantly larger than the average Ge displacement in the glass structure, while also the other, 5-coordinated, Ge atom (denoted Ge_2) undergoes a displacement of 0.34 Å, which is also appreciably larger than the average value (0.14 Å). In addition, one of the tellurium atoms (denoted as Te_6), which is initially shared between the 5-coordinated (Ge_2) and 6-coordinated (Ge_1) germanium atoms and part of a 4-fold ring, experiences a displacement larger than 1 Å, associated with breaking one of the Ge–Te bonds (Ge_2–Te_6), and hence leading to a rupture of the Ge–Te–Ge–Te ring. The displacements of all the atoms (three Ge and seven Te atoms) that correspond to the geometry of the cluster hosting the mid-gap defect can be seen in **Table S1**.

The application of a high electric field results in the initially 6-coordinated Ge_1 atom becoming 4-coordinated by breaking two of the bonds, Ge_1–Te_1 and Ge_1–Te_5, while the initially 5-coordinated Ge_2 atom becomes 4-coordinated as well, by losing the Ge_2–Te_6 bond. We note that for 5-/6-coordinated Ge atoms, the bonds related to the axial, almost-linear, Te–Ge–Te triatomic configurations are the most polarizable and thereby, potentially, the most susceptible to bond breaking. Very recently, it was reported that these are also the sites where hyperbonding occurs in amorphous chalcogenides [48]. Hence, from the analysis presented here, it seems that a high electric field has a tendency preferentially to break these axial long bonds (viz. Ge_1–Te_1, Ge_2–Te_6), transforming the Ge atoms to 4-coordinated configurations. It is noted that, in this analysis, we consider bond formation to occur between two nearby atoms as long as the interatomic distance between these two atoms is shorter than or equal to 3.2 Å.

In order to assess further the overall effect of the electric field on the local atomic structure of the glass model, the total radial distribution function (RDF) was computed for the initial state of the GST-225 amorphous model *M1*, as well as for the same model after the application of electric fields, with intensities 500, 1000, 1500, 2000 and 2500 kV cm^{-1}, along the ⟨111⟩ direction. The calculated average RDFs are shown in **Fig. S7(a)**; no significant differences can be observed in the overall relaxed glass geometry before and after the application of the external electric fields. Therefore, there are no substantial modifications of the short-range order within the amorphous network overall, while the observed structural transformations in the vicinity of the defect cannot be associated with any melting of the glass structure.

A Bader-charge analysis was performed for the atomic species in the GST-225 glass model *M1* to provide some further, electronic-structure-oriented, information on the structural modifications due to the application of the external electric field. The Bader ionic charges were computed from the total electronic charge density by using the scheme described in Ref. [49]. The average Bader charges (in atomic units) for Ge, Sb and Te atoms are shown in **Fig. S7(b)**, for applied electric fields ranging from 0 to 2500 kV cm^{-1}, and it can be observed that the average values for all three atomic species in the model structure remain almost the same, before and after the application of the electric fields. This supports the argument that the overall relaxed amorphous structure, after the application of high electric fields, does not differ much from the initial glass structure, despite the removal of the mid-gap defect from the band gap and the subsequent delocalization of the state at the conduction-band edge, highlighting that the observed structural modifications have a rather local character.

The distributions of the calculated Bader ionic charges of the glass model *M1*, before and after the application of the 2500 kV

cm^{-1} electric field along the ⟨111⟩ direction, are shown in **Fig. S8**, in which no clear systematic variations can be observed. However, the Bader charges of the particular atoms (three Ge and seven Te atoms), that form the local environment hosting the localized mid-gap state in the zero-field glass model *M1* (Fig. 4**(a)**), do exhibit significant changes associated with the field-driven transformation, as can be seen in **Table S1**. The application of the 2500 kV cm^{-1} electric field leads to a reduction of the Bader charge for the two 5- and 6-coordinated Ge atoms, which reflects the field-induced lowering in their coordination to 4-fold, and the consequent modification of their local environments. Hence, higher-than-threshold electric fields mainly affect the region of the structural motif that hosts the localized mid-gap defect state of the zero-field glassy model.

The average field-induced atomic displacements for Ge, Sb and Te species in the glass model *M1* are shown in **Fig. S9**, for applied electric fields ranging from 0 to 2500 kV cm^{-1}. It can be observed that the atomic displacements for below-threshold intensities (500, 1000 and 1500 kV cm^{-1}) of the electric field (for which the mid-gap state remained unaffected in the band gap) are smaller compared to the atomic displacements for the above-threshold values (2000 and 2500 kV cm^{-1}) of the electric field (for which the mid-gap state was eliminated from the band gap). This comparison of the overall atomic displacements inside the amorphous model highlights further the importance of the atomic relaxations, due to the electric field, on the shift of the defect level towards the bottom of the conduction band.

It should be noted that performing molecular-dynamics (MD) simulations with an applied electric field would be able to provide a more coherent picture about the dynamics inside the amorphous material. However, performing DFT-MD simulations with a periodic electric field in a glassy material, such as GST-225, with a narrow band gap is very challenging. Nevertheless, the geometry optimizations with hybrid-DFT calculations of the amorphous structure, carried out here, give a sense of the spatial atomic movements inside the glass structure due to the application of electric fields, which provide a useful insight, especially with respect to the modification of the atomic environments that host the localized mid-gap states in the glass model, and the subsequent annihilation and delocalization of these electronic states.

3.4. Effect of the electric-field polarization vector on the mid-gap states

The effect of the direction of the polarization vector of the applied external electric field on the mid-gap defect states was investigated by applying electric fields with an intensity both at the lower end of the range of the fields studied here, viz. 500 kV cm^{-1}, and also at the higher end of the range, viz. 2500 kV cm^{-1}, along seven different directions within the amorphous network relative to the cubic simulation cell, namely ⟨001⟩, ⟨010⟩, ⟨100⟩, ⟨011⟩, ⟨101⟩, ⟨110⟩ and ⟨111⟩. We should note, though, that obtaining a complete picture about the effect of the electric-field direction in amorphous structures is an arduous task because of the very computer-intensive nature of these field-related simulations. Nevertheless, we believe that the calculations presented here give an indication of the behavior and provide instructive observations about the elimination of mid-gap electronic states and their subsequent delocalization.

The total densities of states for the relaxed GST-225 glass model *M1*, before and after the application of a 500 kV cm^{-1} electric field along the seven different directions, are shown in **Figs. S10–S16**. In all cases, the applied electric field does not affect significantly the mid-gap electronic state of the glassy model, since the defect state maintains its position in the band gap. In contrast, the results of the application of a 2500 kV cm^{-1} electric field along the seven different directions indicate a systematic effect with respect to the elimination of the mid-gap electronic state from the band gap. For all the electric-field polarization vectors studied here, the mid-gap defect state was removed from the electronic structure and transformed into a conduction-band-edge tail state, as shown in **Figs. S17–S23**. Hence, the intensity of the applied electric field seems to play a more critical role than its polarization-vector direction, relative to the orientation of the defect atomic environment hosting the mid-gap state in the simulation cell, with respect to the elimination of the electronic state from the band gap of the glass, at least for the electric fields studied here.

The total electronic densities of states before and after the application of a 2500 kV cm^{-1} electric field, along the ⟨001⟩ direction within the amorphous network, for the GST-225 model *M1,* are presented in Fig. 6(a) for comparison with Fig. 1(a) for the case of the ⟨111⟩ direction. It can be observed, as discussed above, that the electric field has a strong effect on the electronic structure of the glass, by removing the mid-gap defect from the band gap and turning it into a conduction-band-edge electronic state (the transformation is highlighted by the brown dashed arrow). The effect of the electric-field polarization vector on the localization of the electronic state needs to be addressed also here, together with any correlation with possible changes in the atomic geometry of the mid-gap defect. The molecular orbital of, and the atomic geometry hosting, the newly formed conduction-band-tail state, after the application of the external electric field along the ⟨001⟩ direction, are shown in Fig. 6**(b)**. The previously localized mid-gap defect state (see Fig. 3**(a)**) becomes a highly delocalized electronic state in the periodic cell of the amorphous structure. The black dashed frame highlights the atomic geometry of the two Ge atoms that previously formed the structural motif which hosted the mid-gap state. A comparison with their initial local environments (see Fig. 4**(a)**) indicates that their atomic geometry has been significantly modified, since the previously 6- and 5-coordinated Ge atoms become 4- and 3-coordinated, respectively, while the 4-fold ring is ruptured. A comparison with the effect of the 2500 kV cm^{-1} electric field along the ⟨111⟩ direction (see Fig. 4**(c)**) shows that both applied electric fields delocalize the initial mid-gap electronic state. However, the two electric fields, applied in different directions, modify the initial atomic geometry of the mid-gap defect in rather different ways; nevertheless, a common feature is the lowering of the coordination number for the two Ge atoms involved.

The strong connection between electron (de)localization and atomic geometry of the host motif of the electronic state is also highlighted by visualization of the molecular orbital after the application of a 2500 kV cm^{-1} electric field along the ⟨011⟩ direction within the amorphous network, shown in **Fig. S24**. Although the mid-gap state has been removed from the band gap of the glassy model (see **Fig. S20**), a strong spatial localization is maintained for the newly formed conduction-band-edge electronic state. An inspection of the atomic geometry that hosted the initial mid-gap defect reveals that it has not changed significantly after the application of the high electric field along the ⟨011⟩ direction, since a 5-coordinated Ge atom and the 4-fold ring structure remained in the relevant local hosting environment. This indicates that the degree of spatial localization of the electronic state is strongly correlated with the atomic geometry of the original mid-gap state, and it supports the above, similar, observations from the results for different intensities of the electric field applied along a given direction within the glass network.

3.5. Structural relaxation of the amorphous models

It has been previously observed that GST-225 glass models with additional electronic states in their band gap have a higher total energy than do models with a “clean” band gap, indicating that the

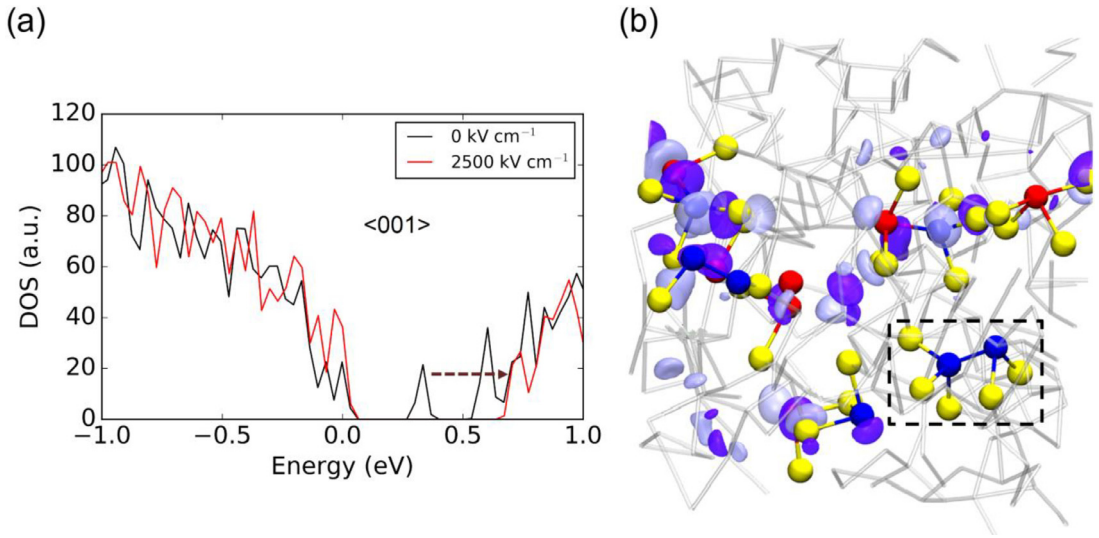

Fig. 6. Effect of electric-field polarization vector on the mid-gap states. (a) Total electronic densities of states (DOS) near the top of the valence band and the bottom of the conduction band before and after the application of a 2500 kV cm^{-1} periodic electric field along the ⟨001⟩ direction for the GST-225 glass model *M1*. The mid-gap defect state is eliminated from the electronic structure and transformed into a conduction-band-minimum tail state, as highlighted with the brown dashed arrow. (b) Atomic structure and molecular orbital of the respective conduction-band-edge state. The application of the high electric field results in a delocalized electronic state. This is accompanied by significant modifications in the atomic geometry (shown inside the black dashed frame) that hosted the original mid-gap defect within the amorphous network. Ge atoms are blue, Sb are red, and Te are yellow. The atomic bonds in the rest of the amorphous network are rendered in gray. The purple and blue isosurfaces depict the molecular-orbital-wavefunction amplitude of the electronic state, and are plotted with isovalues of +0.015 and -0.015, respectively (For interpretation of the references to color in this figure legend, the reader is referred to the web version of this article).

glassy structures with in-gap defect states tend to be less favorable from an energetic perspective [21]. In this study, the energy difference of the model structures before and after the application of the threshold electric fields was computed to get an indication of the degree of structural relaxation due to the shift of the localized in-gap states towards the bottom of the conduction band.

The calculated total energies of the relaxed glass model *M1* after the application of the 2500 kV cm^{-1} electric field along the ⟨001⟩, ⟨010⟩, ⟨100⟩, ⟨011⟩, ⟨110⟩, ⟨101⟩ and ⟨111⟩ directions, that led to the elimination of the mid-gap defect from the electronic structure of the amorphous model (see **Figs. S17–S23**), are lower by 3.23 eV, 1.16 eV, 1.51 eV, 0.53 eV, 0.61 eV, 1.94 eV and 0.13 eV, respectively, compared to the total energy of the relaxed ground state of the zero-field model structure. Moreover, the application of the 2000 kV cm^{-1} electric field along the ⟨111⟩ direction, which also removed the mid-gap state (see **Fig. S4(d)**), resulted in a configuration which was lower in energy by 0.12 eV. It is interesting to highlight that, for the same glass model, the variations in the lowering of the energy among the different applied electric fields stems from the fact that the structural modification of the local motif that was hosting the defect was different after the application of electric fields with different polarization-vector directions (⟨111⟩ vs. ⟨001⟩, for instance).

The calculated total energy of the relaxed glass model *M3* after the application of the 2500 kV cm^{-1} electric field, which removed both the mid-gap and shallow defect states from the band gap, is lower by 1.31 eV compared to the total energy of the relaxed ground state of the zero-field model structure. Finally, in the amorphous model *M2*, the threshold electric field (3500 kV cm^{-1}) eliminated the shallow defect from the band gap of the glass and resulted in a structure which was lower in energy by 2.73 eV.

The calculated energy differences, in the three glass models studied here, highlight that the electric-field-induced elimination of mid-gap defect states leads to structural relaxation of the amorphous structure. Zipoli et al. [17] reported that the annihilation of structural defects from the band gap of amorphous GeTe results in a lower-energy model structure by approximately 1.0 eV, while even larger energy differences have been reported by Raty et al. [15] upon structural relaxation, also in models of glassy GeTe. Hence, from an energetic point of view, aging of the amorphous state in chalcogenide glasses is accompanied by a substantial energy lowering of the model system, which is also the case in our GST-225 model glassy structures, where the energy difference before and after the application of the threshold electric field is significant.

The defect-state annihilation from the band gap of amorphous GeTe upon thermal annealing has been correlated with the breaking of stretched Ge–Te bonds [17,18]. A lowering in the local coordination due to the breaking of unfavorable Ge–Ge bonds in models of amorphous GeTe has been also associated with the structural relaxation of this glassy material [15]. In addition, atomic rearrangements related to the removal of residual resonant-like bonding from the amorphous network have been suggested as being responsible for the structural relaxation of amorphous phase-change materials [50].

In this study, we demonstrated how the weak, polarizable bonds in 5-coordinated Ge atoms within the GST-225 amorphous structure can break under the application of high electric fields, resulting in the engineered (i.e. without thermal annealing) annihilation of mid-gap defect electronic states and the sequential structural relaxation of the glassy model systems. This is in accordance with the experimentally reported electric-field-induced acceleration of the spontaneous structural relaxation in amorphous phase-change memory materials [19]. It is worth mentioning that the threshold electric fields used here, which lead to the observed bond breaking in the amorphous models, are considerably lower in intensity (by more than one order of magnitude) than the fields reported for bond dissociation in water [51] or crystalline MgO [52], for instance.

4. Summary and conclusions

In this study, the Berry-phase formalism, within the modern theory of polarization, has been utilized to apply external, finite, periodic electric fields to glassy models of the phase-change memory material, $Ge_2Sb_2Te_5$ (GST-225). Hybrid-DFT calculations were

employed to optimize the geometry of the amorphous models, before and after the application of the electric fields, and to calculate their electronic structure, in order to shed light on the effect of the applied electric fields on localized mid-gap defect electronic states present in the glassy GST-225 material.

The application of a sufficiently high external electric field removes mid-gap defect states from the band gap of the GST-225 glass and transforms them into electronic states lying at the bottom of the conduction band, as a result of the electric-field-induced atomic relaxations of the amorphous structure. The degree of spatial localization of these newly formed conduction-band-edge states is strongly governed by the atomic geometry that hosts the original mid-gap state. If the applied electric field is below the threshold needed to modify significantly the structural motif that is hosting the defect, then the electronic state, even though it is pushed to the bottom of the conduction band, maintains a strongly localized character. Only above-threshold values of the electric-field intensity, combined with an appropriate direction of its polarization vector relative to the orientation of the defect atomic geometry in the simulation box, and which are sufficient to change the local bonding environment of 5- and 6-coordinated Ge atoms, responsible for the spatial localization of the mid-gap defects in amorphous GST-225, are able to transform the translated electronic state in the conduction-band tail to a delocalized state. Therefore, an appropriate field-induced lowering of the coordination number of Ge atoms, i.e. to become 4-coordinated, as well as breaking of 4-fold (Ge–Te–Ge–Te) rings, seem to be essential for delocalization of conduction-band-edge states.

Understanding the effect of an external electric field on the electronic structure of chalcogenide materials, in particular amorphous GST-225, is imperative for the design of phase-change memory devices with improved performance. The calculations presented in this study link changes in the electronic density of states to modifications in the local atomic structure of the glass, and establish the necessary conditions that are required for localized mid-gap electronic states to be eliminated from the band gap and become delocalized conduction-band-edge states.

Consequently, the present results provide significant insights, that blend both electronic and structural aspects, into the atomistic picture of the effect of an applied electric field on the localized mid-gap defect states in amorphous phase-change memory materials, while they also provide statistical confirmation of the specific modifications in the local environment of the atomic geometry hosting the defect which lead to structural relaxation of the glassy model systems.

In summary, a suitable materials-engineering concept has been demonstrated, where the application of an electric field can be utilized for controlling the distribution of localized states within the band gap of a chalcogenide glassy structure, by tailoring its electronic and atomic structures accordingly, in order to tune the extent of the band tails. Our finding can be useful for potentially mitigating time-dependent resistance “drift” in phase-change memory devices, thereby facilitating the realization of multi-level storage operation in future PCRAM devices. Moreover, this study provides a general example for electric-field tuning of the amorphous structure (state) of functional materials.

Declaration of Competing Interest

The authors declare that they have no known competing financial interests or personal relationships that could have appeared to influence the work reported in this paper.

Acknowledgments

Via our membership of the UK’s HEC Materials Chemistry Consortium, which is funded by EPSRC (EP/L000202, EP/R029431), this work used the ARCHER UK National Supercomputing Service (http://www.archer.ac.uk). K.K. and J.A. acknowledge financial support from the Academy of Finland project No. 322832 “NANOIONICS”.

Supplementary materials

Supplementary material associated with this article can be found, in the online version, at doi:10.1016/j.actamat.2021.117465.

References

[1] M. Wuttig, Towards a universal memory? Nat. Mater. 4 (2005) 265.
[2] Y. Wang, Y. Zheng, G. Liu, T. Li, T. Guo, Y. Cheng, S. Lv, S. Song, K. Ren, Z. Song, Scandium doped $Ge_2Sb_2Te_5$ for high-speed and low-power-consumption phase change memory, Appl. Phys. Lett. 112 (2018) 133104.
[3] R.F. Freitas, W.W. Wilcke, Storage-class memory: the next storage system technology, IBM J. Res. Dev. 52 (2008) 439.
[4] P. Noé, C. Vallée, F. Hippert, F. Fillot, J.Y. Raty, Phase-change materials for non-volatile memory devices: from technological challenges to materials science issues, Semicond. Sci. Technol. 33 (2018) 013002.
[5] R. Bez, A. Pirovano, Non-volatile memory technologies: emerging concepts and new materials, Mater. Sci. Semicond. Process. 7 (2004) 349.
[6] S. Raoux, W. Welnic, D. Ielmini, Phase change materials and their application to nonvolatile memories, Chem. Rev. 110 (2010) 240.
[7] A. Pirovano, A.L. Lacaita, F. Pellizzer, S.A. Kostylev, A. Benvenuti, R. Bez, Low-field amorphous state resistance and threshold voltage drift in chalcogenide materials, IEEE Trans. Electron Devices 51 (2004) 714.
[8] D. Ielmini, S. Lavizzari, D. Sharma, A.L. Lacaita, Temperature acceleration of structural relaxation in amorphous $Ge_2Sb_2Te_5$, Appl. Phys. Lett. 92 (2008) 193511.
[9] M. Boniardi, D. Ielmini, Physical origin of the resistance drift exponent in amorphous phase change materials, Appl. Phys. Lett. 98 (2011) 243506.
[10] J. Luckas, D. Krebs, S. Grothe, J. Klomfaß, R. Carius, C. Longeaud, M. Wuttig, Defects in amorphous phase-change materials, J. Mater. Res. 28 (2013) 1139.
[11] M. Kaes, M. Salinga, Impact of defect occupation on conduction in amorphous $Ge_2Sb_2Te_5$, Sci. Rep. 6 (2016) 31699.
[12] J. Luckas, D. Krebs, M. Salinga, M. Wuttig, C. Longeaud, Investigation of defect states in the amorphous phase of phase change alloys GeTe and $Ge_2Sb_2Te_5$, Phys. Status Solidi C 7 (2010) 852.
[13] D. Krebs, R.M. Schmidt, J. Klomfaβ, J. Luckas, G. Bruns, C. Schlockermann, M. Salinga, R. Carius, M. Wuttig, Impact of DoS changes on resistance drift and threshold switching in amorphous phase change materials, J. Non Cryst. Solids 358 (2012) 2412.
[14] D. Krebs, T. Bachmann, P. Jonnalagadda, L. Dellmann, S. Raoux, Changes in electrical transport and density of states of phase change materials upon resistance drift, New J. Phys. 16 (2014) 043015.
[15] J.Y. Raty, W. Zhang, J. Luckas, C. Chen, R. Mazzarello, C. Bichara, M. Wuttig, Aging mechanisms in amorphous phase-change materials, Nat. Commun. 6 (2015) 7467.
[16] S. Gabardi, S. Caravati, G.C. Sosso, J. Behler, M. Bernasconi, Microscopic origin of resistance drift in the amorphous state of the phase-change compound GeTe, Phys. Rev. B 92 (2015) 054201.
[17] F. Zipoli, D. Krebs, A. Curioni, Structural origin of resistance drift in amorphous GeTe, Phys. Rev. B 93 (2016) 115201.
[18] M.L. Gallo, D. Krebs, F. Zipoli, M. Salinga, A. Sebastian, Collective structural relaxation in phase-change memory devices, Adv. Electron. Mater. 4 (2018) 1700627.
[19] P. Fantini, M. Ferro, A. Calderoni, Field-accelerated structural relaxation in the amorphous state of phase change memory, Appl. Phys. Lett. 102 (2013) 253505.
[20] N.F. Mott, E.A. Davis, R.A. Street, States in the gap and recombination in amorphous semiconductors, Philos. Mag. 32 (1975) 961.
[21] K. Konstantinou, F.C. Mocanu, T.H. Lee, S.R. Elliott, Revealing the intrinsic nature of the mid-gap defects in amorphous $Ge_2Sb_2Te_5$, Nat. Commun. 10 (2019) 3065.
[22] F.C. Mocanu, K. Konstantinou, T.H. Lee, N. Bernstein, V.L. Deringer, G. Csányi, S.R. Elliott, Modeling the phase-change memory material, $Ge_2Sb_2Te_5$, with a machine-learned interatomic potential, J. Phys. Chem. B 122 (2018) 8998.
[23] J. Akola, R.O. Jones, Structural phase transitions on the nanoscale: the crucial pattern in the phase-change materials $Ge_2Sb_2Te_5$ and GeTe, Phys. Rev. B 76 (2007) 235201.
[24] J. Hegedüs, S.R. Elliott, Microscopic origin of the fast crystallization ability of Ge– Sb–Te phase-change memory materials, Nat. Mater. 7 (2008) 399.
[25] R.D. King-Smith, D. Vanderbilt, Theory of polarization of crystalline solids, Phys. Rev. B 47 (1993) 1651.
[26] D. Vanderbilt, R.D. King-Smith, Electric polarization as a bulk quantity and its relation to surface charge, Phys. Rev. B 48 (1993) 4442.
[27] I. Souza, J. Íñiguez, D. Vanderbilt, First-principles approach to insulators in finite electric fields, Phys. Rev. Lett. 89 (2002) 117602.
[28] P. Umari, A. Pasquarello, Ab initio molecular dynamics in a finite homogeneous electric field, Phys. Rev. Lett. 89 (2002) 157602.
[29] J. VandeVondele, M. Krack, F. Mohamed, M. Parrinello, T. Chassaing, J. Hutter, Quickstep: fast and accurate density functional calculations using a mixed Gaussian and plane waves approach, Comput. Phys. Commun. 167 (2005) 103.

[30] G. Lippert, J. Hutter, M. Parrinello, A hybrid Gaussian and plane wave density functional scheme, Mol. Phys. 92 (1997) 477.
[31] J. VandeVondele, J. Hutter, Gaussian basis sets for accurate calculations on molecular systems in gas and condensed phases, J. Chem. Phys. 127 (2007) 114105.
[32] S. Goedecker, M. Teter, J. Hutter, Separable dual-space Gaussian pseudopotentials, Phys. Rev. B 54 (1996) 1703.
[33] M. Guidon, J. Hutter, J. VandeVondele, Robust periodic Hartree-Fock exchange for large-scale simulations using Gaussian basis sets, J. Chem. Theory Comput. 5 (2009) 3010.
[34] K. Konstantinou, T.H. Lee, F.C. Mocanu, S.R. Elliott, Origin of radiation tolerance in amorphous $Ge_2Sb_2Te_5$ phase-change random-access memory material, Proc. Natl. Acad. Sci. U.S.A. 115 (2018) 5353.
[35] M. Guidon, J. Hutter, J. VandeVondele, Auxiliary density matrix methods for Hartree-Fock exchange calculations, J. Chem. Theory Comput. 6 (2010) 2348.
[36] A.M. El-Sayed, M.B. Watkins, V.V. Afanas'ev, A.L. Shluger, Nature of intrinsic and extrinsic electron trapping in SiO_2, Phys. Rev. B 89 (2014) 125201.
[37] K. Konstantinou, D.M. Duffy, A.L. Shluger, Structure and luminescence of intrinsic localized states in sodium silicate glasses, Phys. Rev. B 94 (2016) 174202.
[38] B.S. Lee, J.R. Abelson, S.G. Bishop, D.H. Kang, B.K. Cheong, K.B. Kim, Investigation of the optical and electronic properties of $Ge_2Sb_2Te_5$ phase change material in its amorphous, cubic, and hexagonal phases, J. Appl. Phys. 97 (2005) 093509.
[39] T. Kato, K. Tanaka, Electronic properties of amorphous and crystalline $Ge_2Sb_2Te_5$ films, Jpn. J. Appl. Phys. 44 (2005) 7340.
[40] S.M. Sze, K.K. Ng, Physics of Semiconductor Devices, John Wiley & Sons, Inc., New Jersey, 2006 3rd ed..
[41] J. Dong, D.A. Drabold, Band-tail states and the localized-to-extended transition in amorphous diamond, Phys. Rev. B 54 (1996) 10284.
[42] R. Mazzarello, S. Caravati, S. Angioletti-Uberti, M. Bernasconi, M. Parrinello, Signature of tetrahedral Ge in the Raman spectrum of amorphous phase-change materials, Phys. Rev. Lett. 104 (2010) 085503.
[43] J. Strand, M. Kaviani, D. Gao, A.M. El-Sayed, V.V. Afanas'ev, A.L. Shluger, Intrinsic charge trapping in amorphous oxide films: status and challenges, J. Phys. Condens. Matter 30 (2018) 233001.
[44] K. Konstantinou, F.C. Mocanu, T.H. Lee, S.R. Elliott, Ab initio computer simulations of non-equilibrium radiation-induced cascades in amorphous $Ge_2Sb_2Te_5$, J. Phys. Condens. Matter 30 (2018) 455401.
[45] S. Clima, et al., Ovonic threshold-switching Ge_xSe_y chalcogenide materials: stoichiometry, trap nature, and material relaxation from first principles, Phys. Status Solidi RRL 14 (2020) 1900672.
[46] É.A. Lebedev, N.A. Rogachev, Conductivity of glassy chalcogenide semiconductors in high electric fields, Sov. Phys. Semicond. 15 (1981) 876.
[47] D. Krebs, S. Raoux, C.T. Rettner, G.W. Burr, M. Salinga, M. Wuttig, Threshold field of phase change memory materials measured using phase change bridge devices, Appl. Phys. Lett. 95 (2009) 082101.
[48] T.H. Lee, S.R. Elliott, Chemical bonding in chalcogenides: the concept of multicenter hyperbonding, Adv. Mater. 32 (2020) 2000340.
[49] G. Henkelman, A. Arnaldsson, H. Jónnson, A fast and robust algorithm for Bader decomposition of charge density, Comput. Mater. Sci. 36 (2006) 354.
[50] P. Fantini, M. Ferro, A. Calderoni, S. Brazzelli, Disorder enhancement due to structural relaxation in amorphous $Ge_2Sb_2Te_5$, Appl. Phys. Lett. 100 (2012) 213506.
[51] A.M. Saitta, F. Saija, P.V. Giaquinta, Ab initio molecular dynamics study of dissociation of water under an electric field, Phys. Rev. Lett. 108 (2012) 207801.
[52] A.M. El-Sayed, M.B. Watkins, T. Grasser, A.L. Shluger, Effect of electric field on migration of defects in oxides: vacancies and interstitials in bulk MgO, Phys. Rev. B 98 (2018) 064102.